Decoupled Direct Power Compensators for a Dual-Inverter Based UPFC

Joaquim Monteiro
UnIRE, ISEL, Polytechnic University of Lisbon, Lisboa, Portugal
INESC-ID Lisboa, Portugal
joaquim.monteiro@isel.pt

J. Fernando Silva
DEEC, IST, Universidade de Lisboa, Lisboa, Portugal
INESC-ID Lisboa, Portugal
fernando.alves@tecnico.ulisboa.pt

Sónia Pinto
DEEC, IST, Universidade de Lisboa, Lisboa, Portugal
INESC-ID Lisboa, Portugal
soniafp@tecnico.ulisboa.pt

V. Fernão Pires
ESTSetúbal, Instituto Politécnico Setúbal, Setúbal, Portugal
INESC-ID Lisboa, Portugal
vitor.pires@estsetubal.ips.pt

2025 14th International Conference on Renewable Energy Research and Applications (ICRERA) | 979-8-3315-9989-8/25/$31.00 ©2025 IEEE | DOI: 10.1109/ICRERA66237.2025.11284221

***Abstract*— In recent decades, Unified Power Flow Controllers (UPFCs) have become essential devices for enhancing the flexibility and controllability of modern electrical transmission networks. These devices facilitate the simultaneous control of local bus voltage and the optimization of power flow within electrical power transmission systems. The multilevel converter capability to operate with high voltage levels while generating low-distortion AC voltages, makes multilevel topologies suitable for UPFCs. Within this framework, this paper presents a novel multilevel converter topology and control strategy specifically designed for UPFC applications. The proposed solution employs a dual inverter topology driven by sliding mode direct power controllers, which are controlled via decoupled Proportional-Integral (PI) compensators. The characteristics, capabilities, and resulting flexibility of the proposed UPFC and control subsystem is validated through a series of simulation tests.**

Keywords— Unified Power Flow Controller (UPFC), dual inverter topology, dual inverter, direct power controller, decoupled Proportional-Integral (PI) compensators.

I. INTRODUCTION

The global increase in electricity demand is exceeding transmission networks capacity. Many existing transmission lines, originally designed for local power distribution and emergency backup, struggle to meet the requirements of liberalized energy markets. Consequently, these lines become critical infrastructures in the management of international power flows. Under such conditions, power transmission systems often operate near their stability limits, making them more vulnerable to the widespread impacts of local faults. In this context, the Unified Power Flow Controller (UPFC) represents one of the most versatile solutions within the family of Flexible AC Transmission Systems (FACTS), utilizing power electronics to provide dynamic and precise control over power flows in transmission networks [1-4].

The UPFC concept, first introduced in the early 1990s, is based on two classical three-phase voltage-source inverters (VSIs) configured in a back-to-back arrangement. Thus, a common DC voltage link is necessary, which requires high-capacitance, high-voltage capacitors. This configuration enables the UPFC to operate as a bidirectional AC-to-AC switching power converter, enabling power flow in both directions between the AC terminals of the two inverters [2]. Since the UPFC introduction extensive research has been undertaken on its converter topologies and on the associated control techniques, focusing on both dynamic and static performance characteristics [5-11]. The UPFC can regulate line parameters such as bus voltage, voltage angle, and line impedance, thereby wielding control over both active and reactive power of a transmission line.

Most control methods for the UPFC rely on linearized power system models, which exhibit slow and cross-coupled dynamic responses concerning both active (P) and reactive (Q) power. This reliance can lead to suboptimal dynamic performance and undesirable instability [7-9]. To mitigate these challenges, non-linear approaches have been proposed to enhance dynamic responses and decouple the power system [10]. Regarding UPFC topologies, reference [11] introduces a novel concept known as matrix converter-based direct power control, which substitutes the two inverters by a single matrix converter (MC). The employed nonlinear robust controllers facilitate improvements in dynamic response and power decoupling through sliding mode control techniques. Additionally, predictive control methods have been applied to the UPFC, demonstrating that predictive control offers a promising solution for power flow applications [12, 13]. Conversely, as indicated in [10], UPFCs utilizing proportional-integral (PI) power control exhibit significant cross-coupling between active and reactive power responses. Consequently, it is essential to eliminate transient cross-coupling and the strong interdependence between active and reactive power responses by implementing decoupled cascaded PI voltage and current controllers [14]. Another aspect concerns the power electronic converter. In this case, the use of multilevel topologies is highly recommended due to the power associated with these systems [15-18]. Furthermore, modular topologies are a very interesting solution for this type of application [19].

This paper introduces a new UPFC topology that employs a dual inverter configuration connected to the power transmission line. The dual inverter system consists of two conventional three-phase, two-level inverters connected to a three-phase transformer featuring an open-winding configuration on the secondary side [20]. This structure enables the generation of nine voltage levels on the AC side. The proposed UPFC concept is realized by connecting two such dual inverter structures in a back-to-back configuration [21]. The dual inverter configuration offers the advantage of multilevel simpler operation, enabling the generation of an AC output phase voltage with up to nine levels [22]. This UPFC concept connects to the transmission line on its AC sides using two coupling transformers, one for shunt connection and one for series connection. To enable control, a power transmission network model incorporating direct power controllers is presented. The dual inverter structure of the UPFC model is applied to the development of decoupled direct power controllers, which manage both active (P) and reactive (Q) power. To design the control system, simplified models of the UPFC are used to create decoupled power controllers [7]. Additionally, sliding mode techniques are included to enhance the UPFC's ride-through capability [23, 24]. The proposed controllers regulate P and Q powers in the transmission line while mitigating cross-coupling and maintaining balanced capacitor DC voltages. The dynamic and steady-state performance of the proposed P, Q controllers are evaluated and analyzed through detailed simulations.

II. Dynamic Modeling of the UPFC Power System

The conventional UPFC employs two classical two-level VSIs connected in a back-to-back configuration. UFC based on multilevel converters also use two multilevel converters, such as the Neutral Point Clamped (NPC) topology, also arranged in a back-to-back manner. This study proposes an alternative approach for the multilevel converter UPFC using dual two-level inverter topologies in a back-to-back connection. Fig. 1 illustrates a block diagram of the proposed UPFC structure. One of the dual inverter structures is linked to the power transmission network through a shunt transformer (T_1), while the other is connected in series with a second transformer (T_2). In this configuration, V_S and V_R represent the sending-end and receiving-end voltages, respectively. The VSIs are connected to a transmission line, characterized by a series inductance and resistance (L and R). This modular multilevel structure distinguishes itself from other UPFC configurations based on multilevel inverters.

Based on power flow theory and as illustrated in Fig. 1, the flow of active and reactive power can be regulated by injecting a voltage (V_C) vector with adjustable magnitude and phase angle through a step-up series coupling open windings transformer (T_2). The shunt converter regulates the necessary active power for the UPFC and typically manages the shunt reactive power. Under steady-state conditions, the active power transfer between the UPFC and the power system approaches zero, signifying a stable DC-link voltage. To derive the dynamic model of the power system for the design of active and reactive power controllers, the balanced three-phase system assumed is represented by an equivalent per-phase circuit of both voltage-source inverters (VSIs) as depicted in Fig. 2. Using this simplified circuit, the dynamics of the three-phase transmission line currents i_j (with j=1,2,3) are expressed as follows:

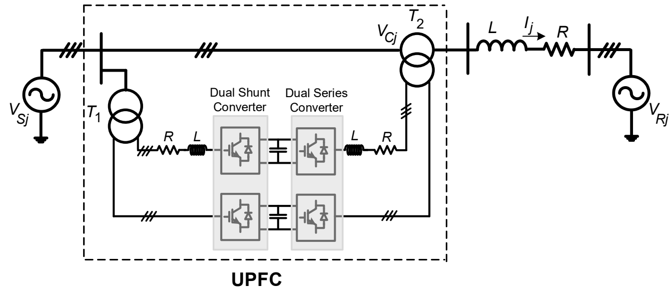

Fig. 1. UPFC with a dual inverter structure.

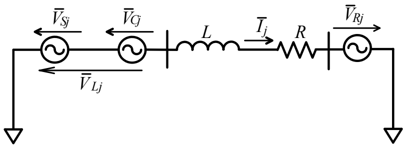

Fig. 2. Per phase equivalent circuit of transmission system with UPFC.

$$\frac{di_j}{dt} = \frac{V_{Sj}+V_{Cj}-Ri_j-V_{Rj}}{L}, \quad with \quad j = 1,2,3 \tag{1}$$

By applying the Park transformation to the equivalent circuit, the AC line current equations in the dq reference frame are derived, as shown in (2):

$$\begin{bmatrix} \frac{dI_d}{dt} \\ \frac{dI_q}{dt} \end{bmatrix} = \begin{bmatrix} -\frac{R}{L} & \omega \\ -\omega & -\frac{R}{L} \end{bmatrix} \begin{bmatrix} I_d \\ I_q \end{bmatrix} + \frac{1}{L} \begin{bmatrix} V_{Ld} - V_{Rd} \\ V_{Lq} - V_{Rq} \end{bmatrix} \tag{2}$$

In (2), the voltages V_{Ld} and V_{Lq} are introduced for notational simplicity, where $V_{Ld}=V_{Sd}+V_{Cd}$ and $V_{Lq}=V_{Sq}+V_{Cq}$. The converter voltages V_{Cd} and V_{Cq}, are obtained by applying Park's transformation to the high voltage measurements at the primary side of the shunt transformer. Thus, by solving (2) in the frequency domain, the system dynamics are expressed as:

$$\begin{bmatrix} I_d(s) \\ I_q(s) \end{bmatrix} = \frac{\begin{bmatrix} sL+R & \omega L \\ -\omega L & sL+R \end{bmatrix}}{(sL+R)^2+(\omega L)^2} \begin{bmatrix} V_{Ld}(s) - V_{Rd}(s) \\ V_{Lq}(s) - V_{Rq}(s) \end{bmatrix} \tag{3}$$

The P and Q powers at line sending side can be expressed in the dq reference frame, by the following equation [25]:

$$\begin{bmatrix} P(s) \\ Q(s) \end{bmatrix} = \begin{bmatrix} V_{Sd}(s) & V_{Sq}(s) \\ V_{Sq}(s) & -V_{Sd}(s) \end{bmatrix} \begin{bmatrix} I_d(s) \\ I_q(s) \end{bmatrix} \tag{4}$$

The proposed UPFC structure is based on a dual-inverter configuration, employing two three-phase, two-level voltage source inverters. Each inverter is connected to the terminals of a shunt transformer with open windings, as shown in the detailed scheme of Fig. 3. In this configuration, the AC-side voltages at the converter inputs are determined by the switching states of the power semiconductors and the levels of the DC voltage sources. Based on the circuit analysis shown in Fig. 3, the dual converter model is derived under the assumption of ideal power switches (S_{ij}), with the switching states represented by the time-dependent variables γ_{ij} (t) where i=1, 2 and j=1,2,3, as defined in (5).

$$\gamma_{ij}\ (t) = \begin{cases} 1, \ if \ \ Sij \ \ is \, ON \ \ and \ \ \bar{S}_{ij} \ \ is \ \ OFF \\ 0, \ if \ \ Sij \ \ is \, ON \ \ and \ \ \bar{S}_{ij} \ \ is \ \ OFF \end{cases} \tag{5}$$

Thus, the three-phase output voltages of the shunt and series dual converters in function of the switch states, are given by (6).

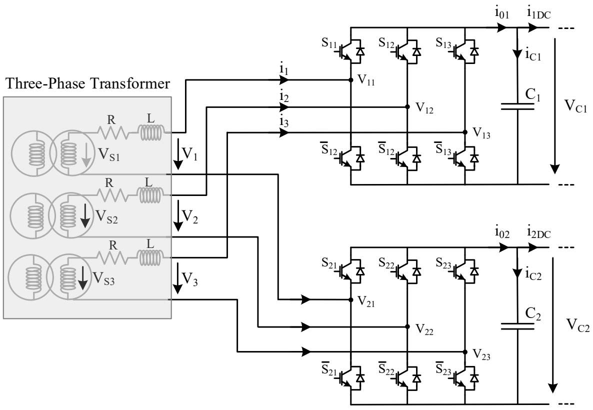

Fig. 3. Dual two-level power converter structure.

$$\begin{bmatrix} V_1 \\ V_2 \\ V_3 \end{bmatrix} = \frac{V_{C1}}{3}\begin{bmatrix} 2 & -1 & -1 \\ -1 & 2 & -1 \\ -1 & -1 & 2 \end{bmatrix}\begin{bmatrix} \gamma_{11} \\ \gamma_{12} \\ \gamma_{13} \end{bmatrix} - \frac{V_{C2}}{3}\begin{bmatrix} 2 & -1 & -1 \\ -1 & 2 & -1 \\ -1 & -1 & 2 \end{bmatrix}\begin{bmatrix} \gamma_{21} \\ \gamma_{22} \\ \gamma_{23} \end{bmatrix} \quad (6)$$

Using the Clark-Concordia matrix transformation defined by (7) on the previous model equations (6), the AC output voltages in the $\alpha\beta$ plane are obtained according (8).

$$\begin{bmatrix} X_\alpha \\ X_\beta \end{bmatrix} = \begin{bmatrix} \sqrt{\frac{2}{3}} & 0 \\ \frac{1}{\sqrt{2}} & \sqrt{2} \end{bmatrix}\begin{bmatrix} X_1 \\ X_2 \end{bmatrix} \quad (7)$$

$$\begin{bmatrix} V_\alpha \\ V_\beta \end{bmatrix} = \begin{bmatrix} \sqrt{\frac{2}{3}} & -\frac{1}{\sqrt{6}} & -\frac{1}{\sqrt{6}} \\ 0 & \frac{1}{\sqrt{2}} & -\frac{1}{\sqrt{2}} \end{bmatrix}\begin{bmatrix} \gamma_{1\alpha} \\ \gamma_{1\beta} \end{bmatrix} V_{C1} - \begin{bmatrix} \sqrt{\frac{2}{3}} & -\frac{1}{\sqrt{6}} & -\frac{1}{\sqrt{6}} \\ 0 & \frac{1}{\sqrt{2}} & -\frac{1}{\sqrt{2}} \end{bmatrix}\begin{bmatrix} \gamma_{2\alpha} \\ \gamma_{2\beta} \end{bmatrix} V_{C2} \quad (8)$$

Based on the previous model equations and considering the allowed switching combinations, 64 distinct voltage space vectors are generated. Assuming equal DC-link capacitor voltages (V_{DC}= V_{C1}= V_{C2}) only 19 of these 64 possible combinations apply distinct AC voltages [21].

By analyzing the AC side of the converters, the dynamic behavior of the dual shunt converters AC currents in phase coordinates (1,2,3) and the capacitor voltages of the converter, as a function of the switch states of the is obtained, resulting in the development of the converter model (9).

$$\begin{bmatrix} \frac{di_1}{dt} \\ \frac{di_2}{dt} \\ \frac{di_3}{dt} \end{bmatrix} = \begin{bmatrix} -\frac{R}{L} & 0 & 0 \\ 0 & -\frac{R}{L} & 0 \\ 0 & 0 & -\frac{R}{L} \end{bmatrix}\begin{bmatrix} i_1 \\ i_2 \\ i_3 \end{bmatrix} - \begin{bmatrix} 2 & -1 & -1 \\ -1 & 2 & -1 \\ -1 & -1 & 2 \end{bmatrix}\begin{bmatrix} \gamma_{11} \\ \gamma_{12} \\ \gamma_{13} \end{bmatrix}\frac{V_{DC}}{3L}$$
$$- \begin{bmatrix} 2 & -1 & -1 \\ -1 & 2 & -1 \\ -1 & -1 & 2 \end{bmatrix}\begin{bmatrix} \gamma_{21} \\ \gamma_{22} \\ \gamma_{23} \end{bmatrix}\frac{V_{DC}}{3L} + \begin{bmatrix} \frac{1}{L} & 0 & 0 \\ 0 & \frac{1}{L} & 0 \\ 0 & 0 & \frac{1}{L} \end{bmatrix}\begin{bmatrix} \gamma_{11} \\ \gamma_{12} \\ \gamma_{13} \end{bmatrix} \quad (9)$$

By applying the Park transformation to the model in phase coordinates (9), the model in the d-q coordinates is obtained. In this formulation, the variables i_d, i_q, γ_{d1}, γ_{q1}, γ_{d2}, γ_{q2}, V_{sd}, and V_{sq} represent the dq frame components, at angular frequency ω, of the original variables i_j, γ_{ij}, and V_{sj}, as shown in (10).

$$\begin{bmatrix} \frac{di_d}{dt} \\ \frac{di_q}{dt} \end{bmatrix} = \begin{bmatrix} -\frac{R}{L} & \omega \\ -\omega & -\frac{R}{L} \end{bmatrix}\begin{bmatrix} i_d \\ i_q \end{bmatrix} + \begin{bmatrix} -1 & 1 \\ -1 & 1 \end{bmatrix}\begin{bmatrix} \gamma_{d1} \\ \gamma_{q1} \end{bmatrix}\frac{V_{DC}}{L} -$$
$$- \begin{bmatrix} -1 & 1 \\ -1 & 1 \end{bmatrix}\begin{bmatrix} \gamma_{d2} \\ \gamma_{q2} \end{bmatrix}\frac{V_{DC}}{L} + \begin{bmatrix} \frac{1}{L} & 0 \\ 0 & \frac{1}{L} \end{bmatrix}\begin{bmatrix} V_{sd} \\ V_{sq} \end{bmatrix} \quad (10)$$

The dynamics of the DC link, can be given by:

$$\begin{bmatrix} \frac{di_d}{dt} \\ \frac{di_q}{dt} \end{bmatrix} = \frac{1}{C}\left[\begin{bmatrix} \gamma_{d1} & \gamma_{q1} \\ \gamma_{d2} & \gamma_{q1} \end{bmatrix}\begin{bmatrix} i_d \\ i_q \end{bmatrix} - \begin{bmatrix} I_{1DC} \\ I_{2DC} \end{bmatrix}\right] \quad (11)$$

Dynamic equations of the phase currents for the dual shunt converters will be used in the design of the UPFC controllers.

III. Design of Decoupled Direct Power Controllers

A. Decoupled of P and Q Power Controllers

The decoupled active and reactive power controllers are derived from (4), assuming that the d-axis of the reference frame is synchronized with the grid voltage, making V_{Sq}=0. Considering V_{Sd} approximately constant and V_{Sq} virtually zero, the expressions for active and reactive power are given in (12).

$$\begin{cases} P(s) = V_{Sd}(s)I_d(s) \\ Q(s) = -V_{Sd}(s)I_q(s) \end{cases} \quad (12)$$

The expressions for active and reactive power in (12), present constant components, ($p_c(s)$ and $q_c(s)$), which are determined by the source voltages and line impedance, as well as dynamic controllable dynamic terms, $\Delta P_C(s)$ and $\Delta Q_C(s)$, determined by the voltages injected by the series converter.

$$\begin{cases} P(s) = p_c(s) + \Delta P_C(s) \\ Q(s) = q_c(s) + \Delta Q_C(s) \end{cases} \quad (13)$$

As indicated in (13), the terms $p_c(s)$ and $q_c(s)$, and the $\Delta P_C(s)$ and $\Delta Q_C(s)$ are defined in (14) and (15), respectively.

$$\begin{bmatrix} p_c(s) \\ q_c(s) \end{bmatrix} = V_{Sd}(s)\frac{\begin{bmatrix} sL+R & -\omega L \\ \omega L & sL+R \end{bmatrix}}{(sL+R)^2+(\omega L)^2}\begin{bmatrix} V_{Sd}(s) - V_{Rd}(s) \\ V_{Rd}(s) \end{bmatrix} \quad (14)$$

$$\begin{bmatrix} \Delta P_C(s) \\ \Delta Q_C(s) \end{bmatrix} = V_{Sd}(s)\frac{\begin{bmatrix} sL+R & \omega L \\ \omega L & -(sL+R) \end{bmatrix}}{(sL+R)^2+(\omega L)^2}\begin{bmatrix} V_{Cd}(s) \\ V_{Cp}(s) \end{bmatrix} \quad (15)$$

To enable fast control response, the multi-input multi-output (MIMO) system can be decoupled by analytically solving the model in (15) for V_{Cd} and V_{Cq}, yielding the inverse dynamic model presented in (16). This formulation reveals that the control inputs V_{Cd} and V_{Cq} are explicitly dependent on the power reference dynamic components.

$$\begin{bmatrix} V_{Cd}(s) \\ V_{Cq}(s) \end{bmatrix} = \frac{1}{V_{Sd}(s)}\begin{bmatrix} sL+R & \omega L \\ \omega L & -(sL+R) \end{bmatrix}\begin{bmatrix} \Delta P_C(s) \\ \Delta Q_C(s) \end{bmatrix} \quad (16)$$

To ensure linear decoupling and zero steady-state error in the closed-loop control of Δ_P and Δ_Q, a first-order decoupled dynamic response with a defined time constant is adopted, as proposed in [10], [14].

$$\begin{bmatrix} \Delta P_C(s) \\ \Delta Q_C(s) \end{bmatrix} = \frac{1}{sT_p+1} \begin{bmatrix} \Delta P_{Cref}(s) \\ \Delta Q_{Cref}(s) \end{bmatrix} \tag{17}$$

Equations for $\Delta P_C(s)$, $\Delta Q_C(s)$ are derived directly from (17).

$$\begin{bmatrix} \Delta P_C(s) \\ \Delta Q_C(s) \end{bmatrix} = \frac{1}{sT_p} \begin{bmatrix} \Delta P_{Cref}(s) - \Delta P_C(s) \\ \Delta Q_{Cref}(s) - \Delta Q_C(s) \end{bmatrix} \tag{18}$$

Next, the expressions for $\Delta_{PC}(s)$ and $\Delta_{QC}(s)$ obtained from (18), are substituted into the inverse dynamic model in (16) to derive the controllers for Δ_P and Δ_Q. The resulting control variables are defined as follows:

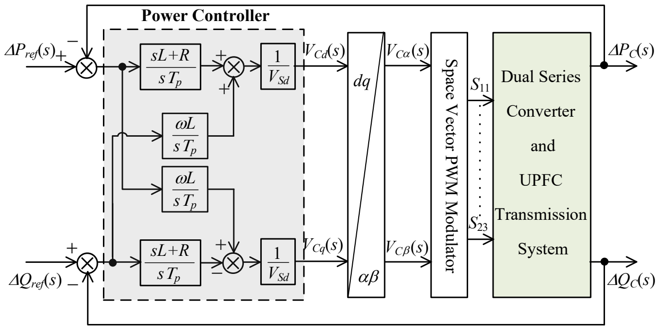

Fig. 4. Block diagram of the decoupled control system for series converter.

$$\begin{bmatrix} V_{Cd}(s) \\ V_{Cq}(s) \end{bmatrix} = \frac{1}{V_{Sd}(s)} \begin{bmatrix} \frac{sL+R}{sT_p} & \frac{\omega L}{sT_p} \\ \frac{\omega L}{sT_p} & -\frac{sL+R}{sT_p} \end{bmatrix} \begin{bmatrix} \Delta P_{Cref}(s) - \Delta P_C(s) \\ \Delta Q_{Cref}(s) - \Delta Q_C(s) \end{bmatrix} \tag{19}$$

Based on this formulation, the decoupled control system is shown in Fig. 4. The power control structure consists of two proportional–integral (PI) loop compensators and two integral cross-coupling compensators, which together enable independent linear control of active and reactive powers, by enforcing the V_{Cd} and V_{Cq} voltages components, using a PWM modulator. These reference voltages are then transformed into a $\alpha\beta$ stationary reference frame and applied to the series converter through space vector PWM modulator.

B. *Design of a Space Vector Controller for the Series Converter*

To control the series dual inverter, a fast and robust voltage regulation strategy based on the sliding mode control (SMC) technique is implemented. Given that the converter switches are operated through the $\alpha\beta$ vectorial modulation scheme, two separate control laws are employed. Thus, by applying the Concordia transformation to the control variables V_{Cd} and V_{Cq}, and averaging $V_{C\alpha}$ and $V_{C\beta}$ over one switching period T, to control the output voltage in the $\alpha\beta$ reference frame. The voltage tracking errors in the $\alpha\beta$ frame are then defined as follows:

$$\begin{cases} e_{C\alpha} = V_{C\alpha ref} - V_{C\alpha} = 0 \\ e_{C\beta} = V_{C\beta ref} - V_{C\beta} = 0 \end{cases} \tag{20}$$

Assuming first-order dynamic behavior for the controller, the evolution of the voltage error components can be expressed as:

$$\begin{cases} \dot{e}_{C\alpha} = \frac{1}{T} e_{C\alpha} \\ \dot{e}_{C\beta} = \frac{1}{T} e_{C\beta} \end{cases} \tag{21}$$

These equations can be written in compact state-space form as:

$$\frac{d}{dt} \begin{bmatrix} e_{C\alpha} \\ e_{C\beta} \end{bmatrix} = \begin{bmatrix} \frac{1}{T} & 0 \\ 0 & \frac{1}{T} \end{bmatrix} \begin{bmatrix} e_{C\alpha} \\ e_{C\beta} \end{bmatrix} \tag{22}$$

Substituting in (22) the error value by expression (20) and solving in order to $V_{C\alpha}$ and $V_{C\beta}$. Then, rearranged and integrated with respect to a generalized time variable τ, resulting in:

$$\begin{bmatrix} V_{C\alpha} \\ V_{C\beta} \end{bmatrix} = -\frac{1}{T} \int \begin{bmatrix} \frac{de_{C\alpha}}{dt} \\ \frac{de_{C\beta}}{dt} \end{bmatrix} d\tau + \begin{bmatrix} V_{C\alpha ref} \\ V_{C\beta ref} \end{bmatrix} \tag{23}$$

This approach represents a feedforward control strategy in which the output voltage is modulated based on the predictive integration of error dynamics.

C. *Control Strategy for the Shunt Converter*

As shown in Fig. 1, the dual shunt converter operates mostly in rectifier mode, supplying active power to the dual series converter, while keeping the common DC bus voltage at its reference value, $V_{DC}=V_{DCref}$. Additionally, the shunt converter is responsible for controlling the reactive power injected at the point of connection. Since the input currents exhibit faster dynamics compared to the slower dynamics of the DC bus voltage V_{DC} the voltage regulation task can be addressed by controlling the reference shunt current I_{dref}, thereby ensuring voltage stability. This control is achieved using a PI controller with proportional and integral gains, denoted by K_{DC} and K_{IV}, respectively.

$$I_{dref} = K_{DC}(V_{DC} - V_{DCref}) + K_{IV} \int_0^T (V_{DC} - V_{DCref})\, dt \tag{24}$$

The reactive power control of the dual shunt converter is performed by regulating I_{qref}, defined as $I_{qref} = -Q_{ref}/V_{Sd}$.

The sliding surfaces used to control the state variables $i_{\alpha,\beta}$, currents, obtained from I_{dref} and I_{qref} through the inverse Park transformation, are defined as follows [23]:

$$S_{\alpha\beta}(e_{i\alpha\beta}, t) = K_{i\alpha\beta}(i_{\alpha\beta ref} - i_{\alpha\beta}) = 0 \tag{25}$$

The convergence of the system will be ensured by the controller, according to a sliding mode stability condition:

$$S_{\alpha\beta}(e_{i\alpha\beta}, t)\dot{S}_{\alpha\beta}(e_{i\alpha\beta}, t) < 0 \tag{26}$$

Fig. 5 shows the block diagram of the control system for the dual shunt inverters.

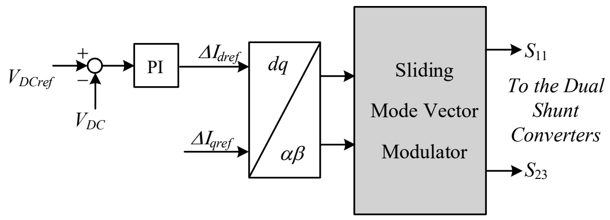

Fig. 5. Block diagram of the control system for the dual shunt converters.

The DC voltage balance of the dual converters will be achieved by using redundant voltage space vectors. To implement this strategy, a vector modulator operating in the $\alpha\beta$ reference frame is employed, as also depicted in Fig. 6.

IV. Simulation Results

To assess the performance of the proposed decoupled power controller applied to the UPFC configuration, a network model, configured with the parameters shown in Fig. 6, was utilized. The power generation units are represented by three-phase synchronous machines equipped with exciters and driven by hydraulic or wind turbines. These machines include governors, power system stabilizers, and output transformers. All components are modeled using the MATLAB/Simulink *SymPowerSystems* toolbox. The dual inverter model was before tested through a laboratory prototype, as in [26].

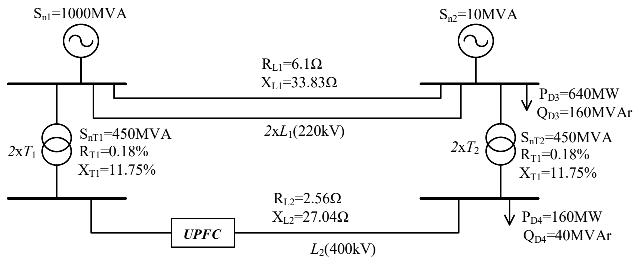

Fig. 6. Network model and parameters used for performance evaluation.

The selected test configuration for the transmission network includes a 220 kV subsystem operating in parallel with a 400 kV subsystem. To assess the proposed controllers, several tests were carried out using detailed simulation models implemented in MATLAB/Simulink. The simulation scenarios were designed to assess the controllers under both steady-state and dynamic conditions, based on transitions in active (P) and reactive (Q) power references.

The following figures present switching simulation results under steady-state conditions. Fig. 7 shows simulated P and Q power flows using the proposed dual-inverter configuration with decoupled direct power controllers. As shown, the controller effectively tracks the power references, with P_{ref} = 240MW and Q_{ref} = 80MVAr. Fig. 8 depicts the corresponding output AC currents at the low-voltage side of the dual series converters, while Fig. 9 shows the capacitor voltages under the same operating conditions. The simulation results confirm that the obtained P and Q power follow the defined references. Additionally, the line currents exhibit a sinusoidal shape, and the proposed voltage balancing strategy for the DC-link capacitors demonstrates satisfactory performance.

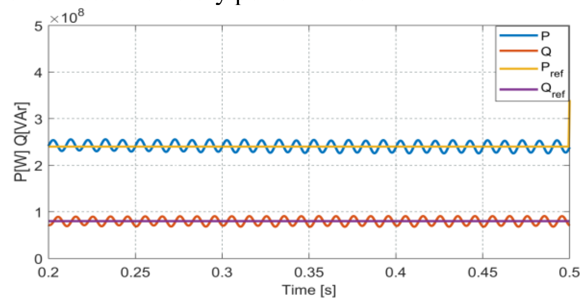

Fig. 7. Active and reactive power flow in the transmission line.

Figs. 10 to 12 present simulation results used to evaluate several system dynamic responses under P and Q power reference transitions. Namely, Fig. 10 illustrates the step response of the P and Q powers in the dual series converters operating as a UPFC controller, subject to reference changes of ΔP_{ref} = 100 MW and ΔQ_{ref} = 50 MVAr. The step changes in P_{ref} and Q_{ref} occur at t = 0.5s and AC currents at the low-voltage side of the dual series converters, while Fig. 12 presents the capacitor voltages under the same operating conditions.

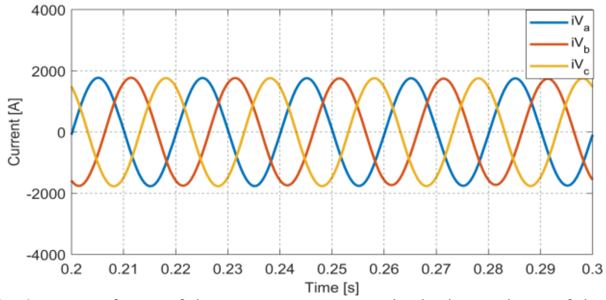

Fig. 8. Waveforms of the output currents AC in the low voltage of the series converters.

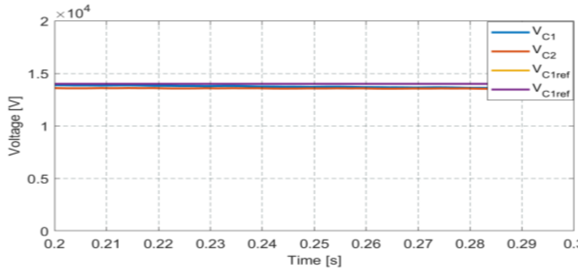

Fig. 9. Waveforms of the capacitors voltages (V_{C1} and V_{C2})

For both power transitions, the tracking performance is nearly ideal, with negligible cross-coupling between the active and reactive power, as each is independently regulated. However, changes in either the active or reactive power setpoints cause the dual series converters, operating as a UPFC, to function with a leading power factor, which results in increased ripple content. Also, the line currents remain close to sinusoidal for both P and Q power transitions. The capacitor voltage equalization is also maintained, even under transient operating conditions.

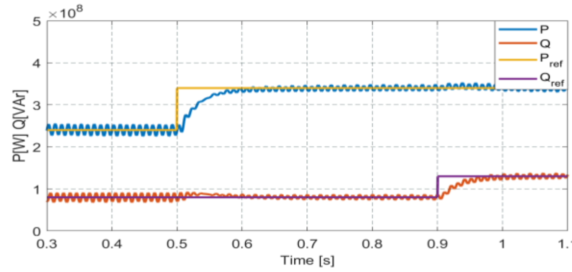

Fig. 10. Active and reactive power response for an P and Q step ($\Delta Pref$=100MW and $\Delta Qref$=50MVAr) respectively in t=0.5s and t=0.9s

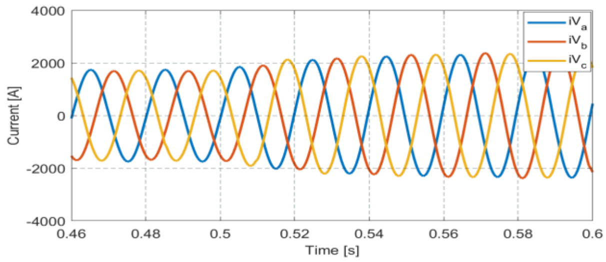

Fig. 11. AC output currents in the low voltage of the series converters for a ΔP_{ref}=100MW and ΔQ_{ref}=50MVAr) respectively in t=0.5s and t=0.9s.

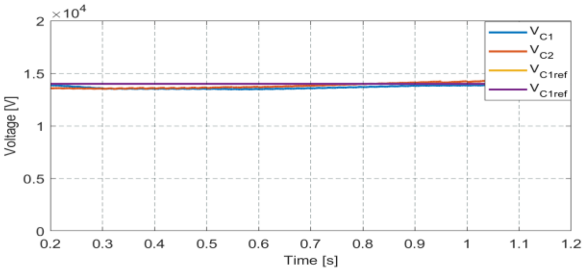

Fig. 12. Waveforms of the capacitors voltages for a ΔP_{ref}=100MW and ΔQ_{ref}=50MVAr, respectively in t=0.5s and t=0.9s).

V. Conclusion

This paper has presented a novel control approach for a UPFC based on dual-inverter multilevel converter topologies. The dual converters are controlled through a sliding mode vector modulator combined with direct power controllers, which are driven by decoupled PI compensators. A dynamic model of the dual-inverter-based UPFC is developed and applied to derive decoupled direct active and reactive power controllers, enabling effective control of active and reactive power flow.

The proposed method enables precise and independent control of active and reactive power by employing decoupled direct power controllers. Simulation results confirm the effectiveness of the strategy, the power flow control, decoupled dynamic behavior, and zero steady-state error. These results validate the suitability of the proposed control scheme for UPFC applications based on dual-inverter structures.

Acknowledgment

This work was supported by UnIRE, ISEL – Polytechnic University of Lisboa and by national funds through Fundação para a Ciência e a Tecnologia, I.P. (FCT) under projects UID/50021/2025 and UID/PRR/50021/2025.

References

[1] Gyugyi, L.,"Unified Power Flow Control Concept for Flexible AC Transmission Systems" *IEE PROCEEDINGS-C*, vol 139, No 4, Jul. 1992.

[2] Gyugyi, L.; Schauder, C.; Williams, S.; Rietman, T.; Torgerson, D.; Edris, A.; "The Unified Power Flow Controller: A New Approach to Power Transmission Control" *IEEE Trans. Power Delivery*, vol. 10, No 2, pp. 1085-1097, Apr. 1995.

[3] Y. -C. Su and P. -T. Cheng, "Design and Evaluation of a Control Scheme for the Hybrid Cascaded Converter based STATCOM with Greatly Reduced Switching Losses," *2024 13th International Conference on Renewable Energy Research and Applications (ICRERA)*, Nagasaki, Japan, 2024, pp. 1322-1329.

[4] M. Chiranj; K. Swarnasri, "Novel Optimization-Based FACTS Devices for Improving the Power Quality in Electrical Distribution Systems" *Intern. Journal of Renewable Energy Research*, vol 12, no 1, March 2022

[5] B. Geethalakshmi and P. Dananjayan, "Investigation of Performance of UPFC without DC Link Capacitor", Electrical Power and Energy Research, Elsevier, 736-746, pp. 284-294, 2008.

[6] K. Wang, L. M. Crow, B. McMillin and S. Atcitty, "A Novel Real-Time Approach to Unified Power Flow Controller Validation" IEEE Trans. Power Systems, vol.25, no.4, pp.1892-1901, Nov. 2010.

[7] J. Monteiro, J. Fernando Silva and S. Pinto, "Matrix converter as unified power flow controller: design and implementation of decoupled direct power controllers,"*9th International Conference on Compatibility and Power Electronics*, Costa da Caparica, Portugal, 2015, pp. 197-201.

[8] T. Ma, "P-Q Decoupled Control Schemes Using Fuzzy Neural Networks for the Unified Power Flow Controller"; Electrical Power and Energy Systems, Elsevier, vol. 29, pp. 748-748, Dec. 2007.

[9] T. Maekawa, T. Takeshita and Y. Kunii, "Node voltage control and line loss suppression using Unified Power Flow Controller on distribution system," *2015 International Conference on Renewable Energy Research and Applications (ICRERA)*, Palermo, Italy, 2015, pp. 1063-1068.

[10] J. Verveckken, F. A. Silva and J. Driesen, "Design of inverse controller with cross-coupling suppression for UPFC series converter", *EUROCON The International Conference on Computer as a Tool*,2007, pp2613-2619.

[11] J. Monteiro, J. F. Silva, S. F. Pinto and J. Palma, "Direct power control of matrix converter based unified power flow controllers," *2009 35th Annual Conference of IEEE Ind. Electron.* Porto, Portugal, 2009, pp. 1525-1530.

[12] B. Ahmadzade, G. Shahgholian, F. M. Tehrani and M. Mahdavian, "Model predictive control to improve power system oscillations of SMIB with fuzzy logic controller," *2011 International Conference on Electrical Machines and Systems*, Beijing, China, 2011, pp. 1-5.

[13] J. Monteiro, J. Silva, S. Pinto and J. Palma; "Inverse Dynamics Based Predictive Control for Unified Power Flow Controllers without DC Bus", *5th International Symposium on Power Electronics For Distributed Generation Systems*, *PEDG´14*, 24-27 June 2014.

[14] N. M. R. Santos, J. F. Silva, J. Verveckken, V. M. F. Pires and R. Castro, "Enhancing the Ride-Through Capability of DC-Link Voltage in NPC Multilevel Unified Power-Flow Controllers" in *IEEE Trans. on Power Delivery*, vol. 29, no. 4, pp. 1542-1550, Aug. 2014.

[15] A. Benevieri, S. Cosso, A. Formentini, M. Marchesoni, M. Passalacqua, L. Vaccaro. "Advances and Perspectives in Multilevel Converters: A Comprehensive Review" *Electronics*, vol. 13, no. 23, p. 4736, Dec. 2024.

[16] V. F. Pires, A. Cordeiro, D. Foito, J. Monteiro, Hao Chen, J. F. Silva, "Modular nine-level single-phase inverter with quadruple voltage gain using reduced blocking voltage switches", e-Prime - Advances in Electrical Engineering, Electronics and Energy, Volume 11, 2025.

[17] H. Kadri, A. Tlemcani, e N. Henini, "Comparison Between the Most Popular Structures of Multilevel Inverters and the Packed U Cell Structure" IJSmartGrid, Vol.7 nº3, 2023.

[18] G. Sorrentino, C. Nevoloso, G. Scaglione, G. Schettino, M. Pastorelii and R. Miceli, "Comparative Analysis Among Multisampling Methods for Three-Phase Grid-Connected Cascaded H- Bridge Multilevel Inverters" *2024 13th International Conference on Renewable Energy Research and Applications (ICRERA)*, Nagasaki, Japan, 2024, pp. 1406-1410

[19] H. Huang, L. Zhang, O. Oghorada and M. Mao, "Analysis and Control of a Modular Multilevel Cascaded Converter-Based Unified Power Flow Controller," *IEEE Trans. Ind. Appl* vol. 57, no. 3, pp. 3202-3213, May-June 2021.

[20] V. F. Pires, D. Foito and J. F. Silva, "Fault-Tolerant Multilevel Topology Based on Three-Phase H-Bridge Inverters for Open-End Winding Induction Motor Drives," *IEEE Transactions on Energy Conversion*, vol. 32, no. 3, pp. 895-902, September 2017.

[21] J. Monteiro, V. F. Pires, J. F. Silva and S. Pinto, "Mutilevel Bipolar Back-to-Back HVDC Transmission System Based on the Dual Inverter Converter Structure with Model Predictive Control" *IECON 2022 - 48th Annual Conf. of the IEEE Industrial Electronics Society*, 2022, pp. 1-6.

[22] G. Grandi, C. Rossi, D. Ostojic and D. Casadei, "A New Multilevel Conversion Structure for Grid-Connected PV Applications," *IEEE Trans. Ind. Electron*, vol. 56, no. 11, pp. 4416-4426, Nov. 2009.

[23] W. Gao and J. Hung, "Variable structure control of nonlinear systems: A new approach," *IEEE Trans. Ind. Electron.*,v40, n 1, pp 45–44, Feb.1993.

[24] José Fernando Silva, Sónia F. Pinto, Linear and Nonlinear Control of Switching Power Converters, Editor(s): Muhammad H. Rashid, Power Electronics Handbook (Fourth Edition), Butterworth-Heinemann, 2018, Pages 1141-1220.

[25] H. Akagi, Y. Kanazawa and A. Nabae, "Instantaneous reactive power compensators comprising switching devices without energy storage components",*IEEE Trans. Ind. Appl.* v. 20, no.3, pp. 625-630, May 1984.

[26] V. Fernão Pires, J. F. Martins, Chen Hao, "Dual-Inverter for Grid-Connected Photovoltaic System: Modeling and Sliding Mode Control", *Solar Energy, Elsevier*, vol. 86, no. 7, pp. 2106-2115, July 2012.